Evaluating Coastal Wetland Mapping Accuracy with High-Resolution Multi-spectral Imagery and LiDAR Remote Sensing Data

Matilda Anokye, Leila Hashemi-Beni

Department of Built Environment, North Carolina A&T State University, 1601 E Market St, Greensboro, NC, USA,

Keywords: Wetlands, Random Forest, LiDAR, Multi-spectral, Classification

Abstract

The coastal area of New Hanover County in North Carolina encompasses diverse wetland habitats influenced by unique coastal and tidal dynamics, with researchers examining the impacts of landscape changes, sea-level rise, and climate fluctuations on wetland health and biodiversity. This study integrates multispectral imagery data, LiDAR, and additional sources to enhance classification accuracy. The study also addresses binary classification for wetland and non-wetland classification and a multi-classification for different wetland classes, leveraging on the Random Forest algorithm which significantly improved the overall accuracy of wetland mapping. The Random Forest model's performance in different scenarios was evaluated, with Scenario 1 achieving an overall accuracy of nearly 93.9%, Scenario 2 achieving an overall accuracy of 93.5%, Scenario 3 achieving an overall accuracy of 94.1%, and Scenario 4 achieving an overall accuracy of 88.2%. These results underscore the model's effectiveness in accurately classifying coastal wetland areas under diverse remote sensing scenarios, highlighting its potential for practical applications in wetland mapping and ecological research.

1. Introduction

1.1 Wetlands

Coastal wetlands are defined by the Coastal Area Management Act (CAMA) as tidally influenced wetlands that contain one or more of the ten salt-tolerant and fresh marsh plant species designed (Carle, 2011). These wetlands play a key role in regional and global environments, and are critically linked to major issues such as climate change, wildlife habitat, biodiversity, water quality protection, and global; carbon and methane cycles (Torres-Bejarano et al., 2021), (Hu et al., 2017), (Bwangoy et al., 2010), (Tiner, 2016), (Ouyang et al., 2014),(Gutzwiller and Flather, 2011), (Mitra et al., 2005).

In coastal areas, wetlands serve as a key source of nutrient cycling capacity to maintain water quality (Childers et al., 2006), peatlands play a key role in carbon sequestration from the atmosphere (Harenda et al., 2018), and mangrove forests are important habitats for many aquatic and terrestrial species (Nagelkerken et al., 2008). In flood mitigation, coastal wetlands act as natural habitats where they can store excess water during flood events and storm damage (Acreman and Holden, 2013),(Michener et al., 1997). For example, the Pantanal wetland in South America can store up to 3 meters of water during the rainy season (Junk and de Cunha, 2005). Despite the many living resources provided by coastal wetlands, people neglect their ecological capacity while simultaneously pursuing high urbanization rates. Between 25 and 50 percent of the world's coastal wetlands were historically converted to farmland or aquaculture in the 20th century, and predictions indicate that the rise of sea level will cause an additional 20 to 45 percent loss this century (Kirwan and Megonigal, 2013). It becomes imperative for the management and conservation of wetlands using various mapping and surveying techniques.

Mapping and monitoring coastal wetlands is particularly challenging due to their complex spatial structure and frequent flooding, which restricts accessibility and complicates traditional survey methods (Kalacska et al., 2017). Shifting tidal waters and dense or overlapping canopy layers further add to the difficulty, especially when mapping forested coastal wetlands. However, technological developments have facilitated the extensive use of remote sensing data for wetland mapping and classification, with improved accuracy. Multispectral and LiDAR systems have been reviewed as the main sensors used in this type of analysis and other environmental management application (Chust et al., 2008), (Rapinel et al., 2015),(Gonzalez-Perez et al., 2022) (Pricope et al., 2024), (Agboola and Beni, 2024), (Blay et al., 2024), (Wasehun et al., 2025), (Hashemi-Beni et al., 2024). LiDAR sensors offer detailed elevation and vegetation structure data, which is crucial for hydrological and ecological studies, while multispectral sensors are especially useful for vegetation classification and soil moisture (Adam et al., 2010), (Hashemi Beni, 2023). However, LiDAR-derived elevation data might vary in accuracy, especially in wetlands with dense vegetation. Notwithstanding these difficulties, the combination of LiDAR and multispectral data has helped to improve wetland delineation and mapping (Carle, 2011). Few studies have thoroughly examined the combined use of its full range of outputs - altimetry, topographically derived features, and intensity data for comprehensive coastal habitat mapping (Anokye et al., 2024) (Lin, 2019), (Ahmed et al., 2015), (Merrick et al., 2013). This study sought to evaluate the combination of multispectral imagery and LiDAR data to accurately map the distribution of wetlands along the coast of New Hanover County in North Carolina.

2. Materials and Methods

2.1 Study Area

The study was conducted in New Hanover County, North Carolina, focusing on coastal wetland ecosystems that play a critical role in the support of biodiversity and the regulation of environmental flows (New Hanover County, 2024). This area en-

This contribution has been peer-reviewed. The double-blind peer-review was conducted on the basis of the full paper.
https://doi.org/10.5194/isprs-annals-X-G-2025-109-2025

compasses diverse wetland habitats influenced by the region’s unique coastal and tidal dynamics, with researchers from various fields examining the impacts of landscape changes, sea - level rise, and climate fluctuations on coastal wetland health and biodiversity (Hilburn, 2024). The study site includes significant estuarine and marsh areas that serve as protected zones, supporting ecosystems services for the local environment and communities (Port City Daily, 2023).

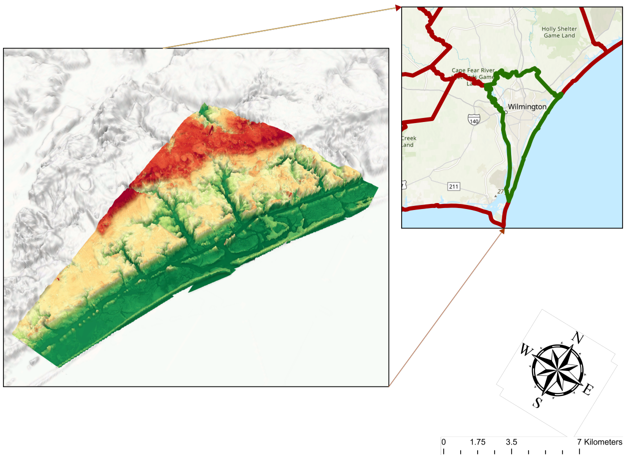

Figure 1. Study Area of coastal New Hanover County located within the Wilmington City in North Carolina.

2.2 Data

We retrieved multispectral data, LiDAR and additional sources of data as explained in subsequent sections.

2.2.1 Predictor Data

Multispectral Imagery - We retrieved multispectral imagery from the National Agricultural Imagery Program (NAIP) and PlanetScope. NAIP captures high-quality-lea-on-data during the growing season with minimal loud cover, offering 1m spatial resolution across red, green, blue and Near-InfraRed bands in a three-year cycle (Mainali et al., 2023). All four bands were included in our model training. PlanetScope data, acquired every five days year round, provided four bands covering Near-Infrared, red, green and blue at a 1m spatial resolution. To capture seasonal and phenological variations in wetland reflectance (Mainali et al., n.d.), Planetscope imagery from spring (March-May), summer(June-August) and Fall(September - November) of 2018, 2019, and 2020 were utilized.

Topographical Data - LiDAR point cloud data classified as ”ground” and ”non-ground” returns were preprocessed to extract (i) intensity image (ii) Digital Surface Model (DSM) (iii) a Digital Terrain Model (DTM) (iv) Canopy Height Model (CHM) expressed relatively to the river level.

Intensity is the return strength of the laser pulse that generated each point, corresponding to the specific spectral wavelength of the emitted laser. It is particularly characterized as the ratio of the reflected light’s strength to that of the emitted light (Chust et al., 2008). Wetland soils especially when saturated, tend to absorb more of the LiDAR pulse than dry areas often resulting in notably can you lower intensity values for wetlands and inundated zones compared to non-inundated surroundings (Mainali et al., 2023). The CHM was created by subtracting the DTM from the DSM. To derive valley bottom features, the DTM was adjusted relative to the river slope, creating a new DTM expressed in terms of river-relative elevation. Both DSM and DTM can improve the detection of forested wetlands that are not distinguishable in the NAIP imagery (Maxwell et al., 2016). All LiDAR-derived images were rasterized at 1m spatial resolution using the nearest neighbor interpolation model to optimize speed and accuracy.

The Canopy Height Model, CHM is given by:

$$CHM = DSM - DTM \tag{1}$$

where DSM = Digital Surface Model
DTM = Digital Terrain Model

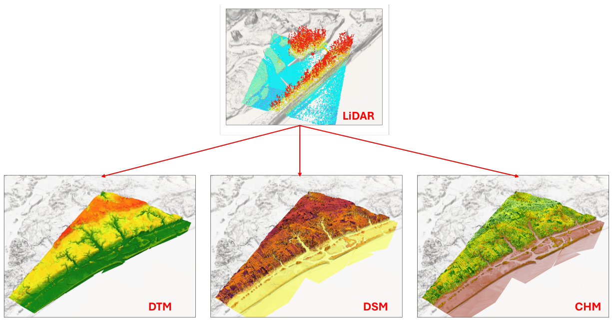

Figure 2. LiDAR Derived Topographic Indices.

Developing Digital Terrain Surface Metrics - Integrating Topographic indices from DTM helps to capture dynamics such as ground water influence, surface flow, and soil moisture distribution (Mohamedou et al., 2019). We extracted Topographic Wetness Index (TWI), Depth To Water (DTW) and Topographical Profile Curvature (TPC). Topographical Wetness Index is calculated using slope and specific catchment area, indicating potential soil moisture levels based on terrain position (Riihimäki et al., 2021). Higher TWI generally correspond to wetter areas TWI has proven useful for detecting areas prone to wetland formation and inundation by estimating hydrologic responsiveness across landscapes. This is defined as

$$\mathrm{TWI} = \ln\left(\frac{\mathrm{a}}{\tan\beta}\right) \tag{2}$$

where $tan(B)$ = the local slope
a = specific catchment area

Depth to Water is a soil moisture index based on the assumption that soils closer to surface water, in terms of distance and elevation , are more likley to be saturated (Mohtashami et al., 2022), (Echiverri and Macdonald, 2019), (Larson et al., 2022). The DTW is defined as

The depth to water D_w is given by:

$$DTW(m) = H_g - H_w \tag{3}$$

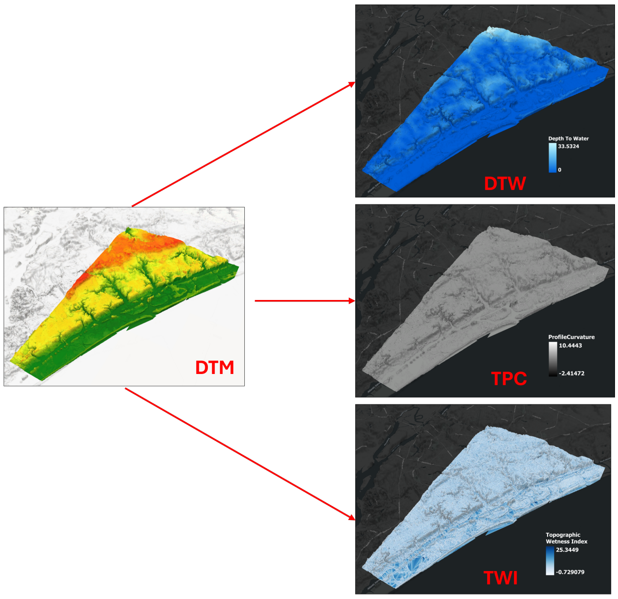

Figure 3. Surface metrics generated from Digital Terrain Model.

where c = principle distance
D_w = depth to the water table
H_g = ground elevation
$H_w Z$ = water table elevation

Topographic Profile Curvature describes the slope curvature of the terrain, influencing water flow, velocity and direction (Halabisky et al., 2022), (Li et al., 2020). Positive values often lead to diverging water flows, while negative values favor converging flows, which are critical in forming saturated areas favorable for wetland. This is defined as

$$K_p = \frac{\partial^2 z}{\partial x^2}\cos^2\theta + \frac{\partial^2 z}{\partial y^2}\sin^2\theta + 2\frac{\partial^2 z}{\partial x \partial y}\sin\theta\cos\theta \tag{4}$$

where c = principle distance
K_p = profile curvature
z = elevation
$xandy$ = horizontal coordinates
= slope aspect angle

In addition to the above LiDAR-derived products, we also created geomorphic landform as an additional predictor dataset based on its recent use in research studies that have increased wetland mapping and classification accuracy (Mainali et al., 2023). Geomorphons are a recent DEM-derived classification that identifies terrain patterns using local elevation relationships. The method integrates measures of openness to define areas as higher, lower, or at the same elevation relative to their surroundings (Mainali et al., n.d.). This classification enables a self-adjusting search that maps terrain features at multiple scales simultaneously, leading to 498 geomorphons that represent common landforms such as valleys, ridges, peaks, and hollows. This highlights the potential of geomorphons for identifying the complex terrain of wetland differentiation (Mainali et al., 2023),

2.2.2 Reference Data

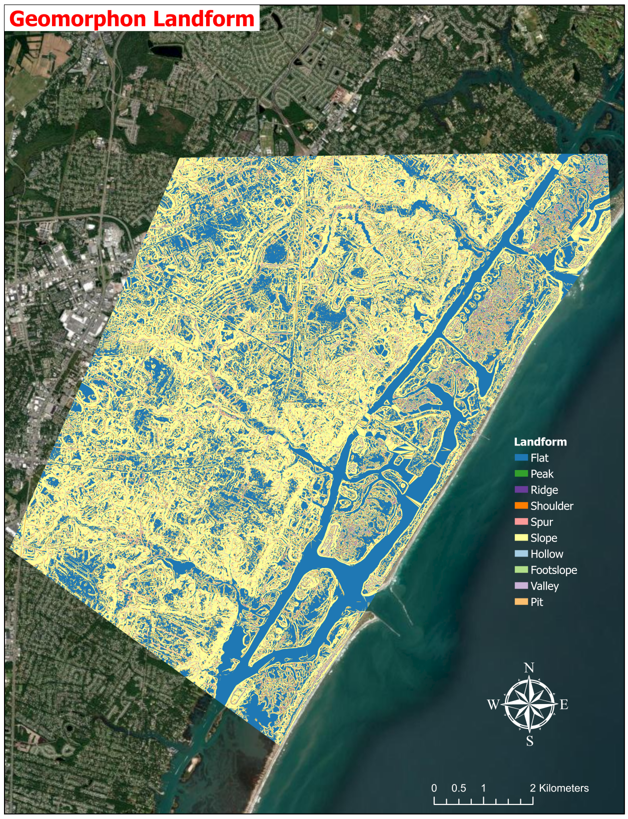

Figure 4. Geomophorn Landform as additional surface metric.

Reference data with accurate georeferencing were sourced from the National Wetland Inventory(NWI) and the North Carolina Coastal Region Evaluation of Wetland Significance(NC-CREWS). NWI data for the study area was downloaded from https://www.fws.gov/program/national-wetlands-inventory/download-state-wetlands-data and the NC-CREWS is available at https://www.deq.nc.gov/about/divisions/coastal-management/coastal-management-gis-data/download-coastal-wetlands-spatialNC-CREWS. All reference wetland data were obtained in vector format and converted into binary rasters, which we refer to as label data.

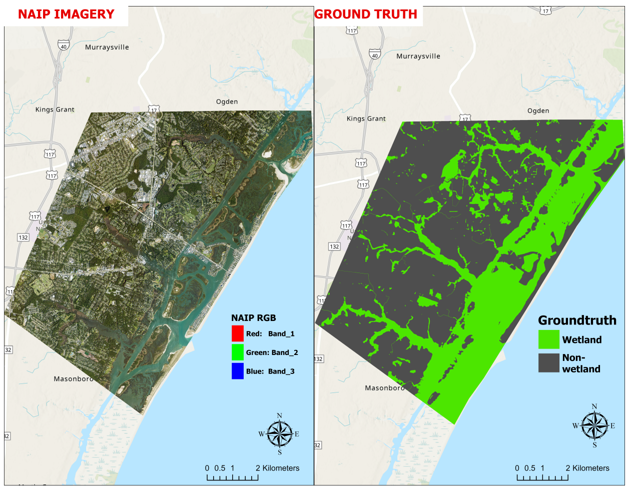

Figure 5. Multispectral NAIP Imagery with the corresponding Groundtruth mask.

2.2.3 Data Pre-processing

We ensured that all data were resampled to a uniform spatial resolution of 1m and properly aligned within the area of interest (AOI). The predictor data and reference data were georeferenced in the North Carolina State Plane - NAD 1983 StatePlane North Carolina FIPS 3200 (Meters)

2.2.4 Random Forest Classification

The Random Forest (RF) model was developed using the predictor input variables. The random forest algorithm was run under four different scenario with different input predictor data for each scenario. This was to assess the relevance of the different input predictor variables in the accuracy of the wetland mapping.

Scenario 1 Under scenario 1, we employed the four bands of the NAIP imagery with the surface metrics (TWI, TPC and DTW) as the predictor variables. Together, these metrics allow the model to leverage topographic and hydrological data for accurate wetland mapping, particularly in areas where soil and vegetation indicators alone may not provide sufficient information.

Scenario 2 Under scenario 2, we employ the topographic indices generated from LiDAR point cloud as additional inputs. That is the Digital Surface Model, Canopy Height Model, Geomorphic Landform, and LiDAR Intensity.

Scenario 3 Under scenario 3, we refined the model by integrating land cover derived datasets such as Sentinel 2 land cover, NDVI and NDWI. Combining these layers allows the Random Forest model to capture distinct spectral and structural features of wetlands, improving its ability to predict their locations with greater precision and reliability.

Scenario 4 Under scenario 4, we employed all the predictor variables with the reference data to perform a multi-classification showing the different wetland classes in the study area using the random forest model.

To evaluate model performance, separate random data subsets were generated for the dependent and independent variables: one subset for model training (the calibration dataset) and another for validation (the target dataset). Model quality was assessed and the final predictions were validated on the full target dataset, with precision, recall and f1-score metrics reported.

3. Results and Discussion

The results and accuracy of the wetland classification using multispectral and LiDAR data are explained below based on each scenario.

3.1 Scenario 1

The integration of only the topographic predictor variables under scenario 1 generated the classified map showing the wetland and upland (non-wetland) classes as shown in Figure 6 with its evaluation performance metrics in Table 1 below.

From Table 1 above, wetland class has a relatively high precision, meaning that most predictions for this class are accurate. However, the recall is slightly lower, suggesting that some instances of wetland class may have been misclassified as other classes. Non-wetland class has a high recall, indicating that the model captures most actual instances of this class. The high f1-score shows a balance between precision and recall, highlighting the model’s effectiveness for this class. The model has a strong overall accuracy across all classes, capturing nearly 94% of cases correctly.

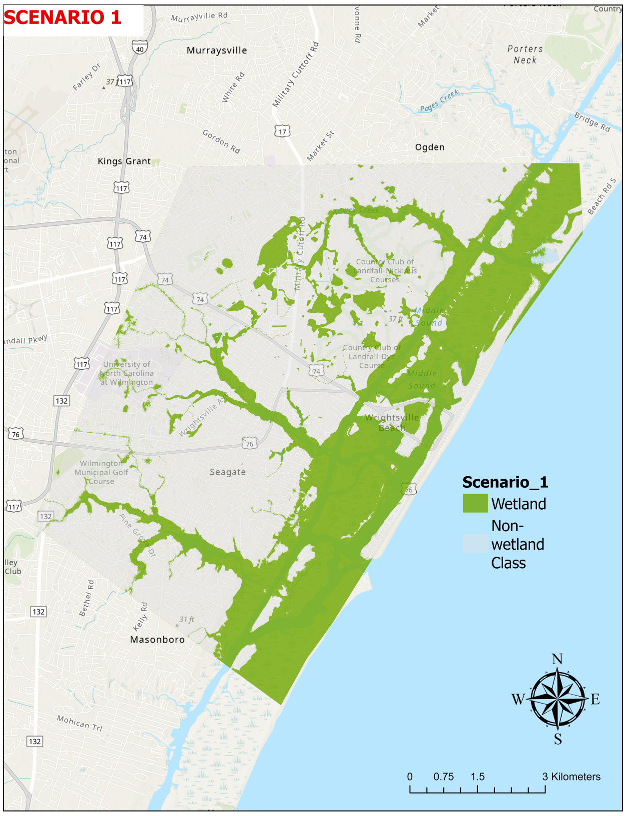

Figure 6. Classified map showing areas of predicted wetland extents under scenario 1

Class	Precision	Recall	F1-score
Wetland	0.952	0.878	0.913
Non-wetland	0.932	0.975	0.953
Accuracy		**0.939**	
macro avg	0.942	0.926	0.933
weighted avg	0.940	0.939	0.938

Table 1. Evaluation metrics for Random Forest classification - Scenario1

3.1.1 Scenario 2

Integrating the Canopy Height Model and LiDAR intensity and the Geomorphic Landform generated the following results as expatiated below. Figure 8 shows the classified map for scenario 2.

Class	Precision	Recall	F1_score
Wetland	0.934	0.885	0.909
Non-wetland	0.935	0.964	0.949
Accuracy		0.935	
macro avg	0.935	0.924	0.929
weighted avg	0.935	0.935	0.935

Table 2. Evaluation metrics for Random Forest classification - Scenario 2

The overall accuracy under scenario 2 is 0.935, indicating the model correctly classifies 93.5% of instances.The high precision and recall for both classes suggest good performance, es-

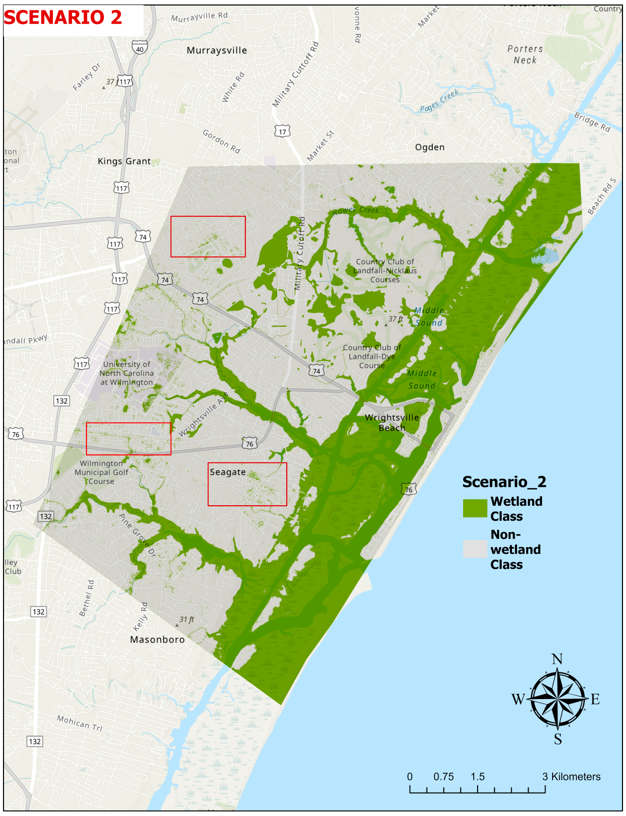

Figure 7. Classified map showing areas of predicted wetland extents under scenario 2 with misclassified pixels shown in the red rectangular red box

pecially for the "Non-wetland" class with a recall of 0.964, indicating a low rate of false negatives. Moreover, the pixels in the red boundary are upland areas that were misclassified as wetland areas.

3.1.2 Scenario 3 Integrating landcover products showed the following outputs as shown in the classified map in Figure 9 and evaluation metrics table in Table 3 below. The overall accuracy under scenario 2 is 0.935, indicating the model correctly classifies 93.5% of instances.The high precision and recall for both classes suggest good performance, especially for the "Non-wetland" class with a recall of 0.964, indicating a low rate of false negatives.

Class	Precision	Recall	F1 Score
Wetland	0.936	0.895	0.915
Non-wetland	0.937	0.967	0.951
Accuracy		0.941	
Macro avg	0.937	0.931	0.933
Weighted avg	0.937	0.941	0.939

Table 3. Evaluation Metrics for the binary RF model under scenario 3

3.1.3 Scenario 4 The results after multiclassification with the RF model are shown in the Classified map in Figure 11, with the evaluation metrics shown in Table 4.

3.1.4 Variable Importance The overall importance of each contributing predictor variable in all scenarios is summarized in Figure 8. The depth to the water was of high importance due to its direct influence on wetland hydrology. Depth To Water which measures the vertical distance from the land surface to

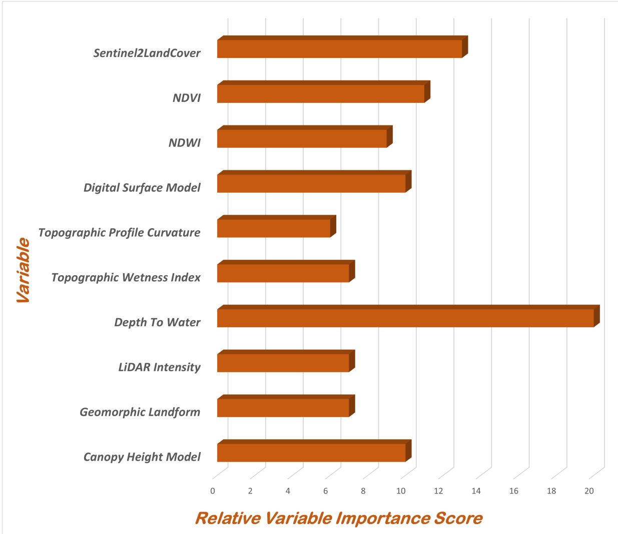

Figure 8. Variable importance of each predictor variable

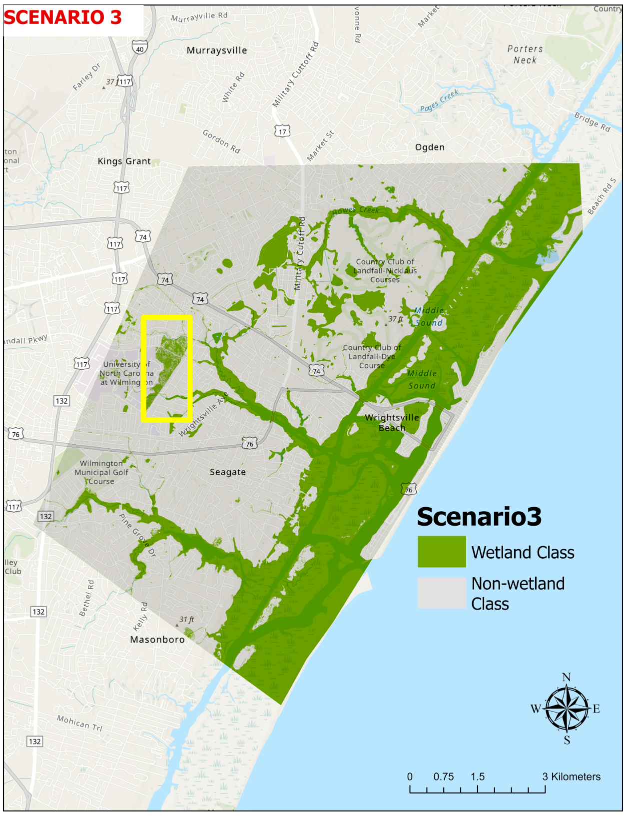

Figure 9. Classified map showing areas of predicted wetland extents with newly predicted areas shown in yellow under scenario 3

the water table, plays a pivotal role in determining soil saturation levels, vegetation types and overall coastal wetland functionality. Other variables such as Sentinel2LandCover, NDVI, NDWI, and Canopy Height Model also highly contributed to the wetland's prediction. Integrating land cover data improved the accuracy of the model by capturing both spectral and structural information. NDWI complemented NDVI, providing additional insight into the moisture status of wetlands. Variations in canopy height indicated the presence of different types of

Class	**Precision**	**Recall**	**F1-score**
Upland	0.969	0.897	0.932
Hardwood Flat	0.348	0.229	0.276
Pine Flat	0.335	0.253	0.288
Salt/Brackish Marsh	0.574	0.947	0.715
Riverine Swamp Forest	0.290	0.411	0.340
Pocosin	0.356	0.300	0.326
Headwater Swamp	0.492	0.171	0.254
Freshwater Marsh	0.429	0.252	0.318
Estuarine Shrub/Scrub	0.207	0.423	0.278
Accuracy		0.882	
Macro avg	0.445	0.432	0.414
Weighted avg	0.908	0.882	0.889

Table 4. Classification Report

wetland.

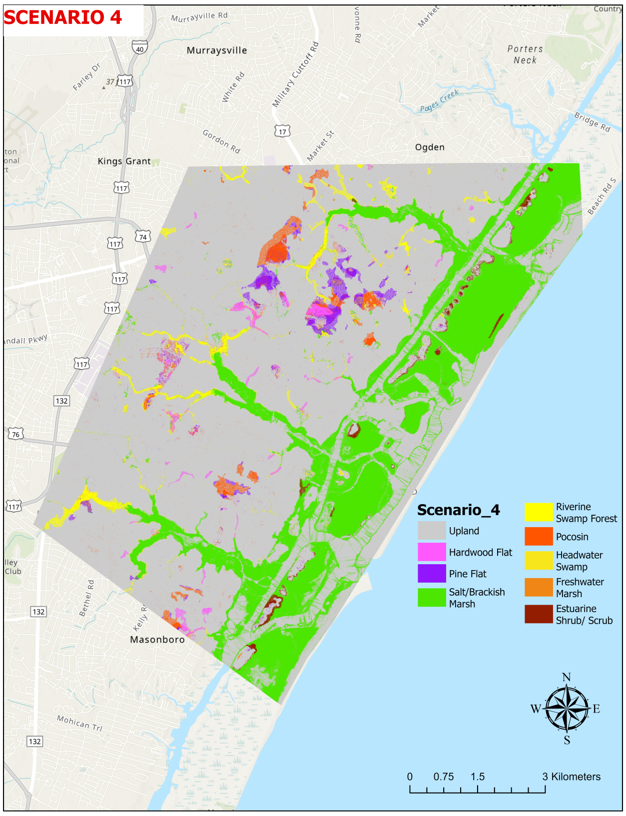

Figure 10. Classified map of different wetland types in the AOI under scenario 4

The model performs across different wetland types, showing it’s generally accurate but struggles with certain classes like ”Estuarine Shrub/Scrub” and ”Hardwood Flat,” which have lower F1-scores due to imbalances in precision and recall. The model performs with an overall accuracy with an F1-score of 82.8%.

3.2 Conclusion and Discussion

The study evaluated the accuracy of Random Forest classification in mapping coastal wetland areas under diverse remote sensing scenarios, focusing on New Hanover County, North Carolina. The research integrated LiDAR, multispectral data, and additional sources to enhance classification accuracy. The results showed that integrating topographic indices from LiDAR point cloud, landcover products such as NDVI and NDWI, and multi-classification with the Random Forest model significantly improved the overall accuracy of wetland mapping. The Random Forest model’s performance in each scenario was evaluated based on precision, recall, F1-score, and overall accuracy. In Scenario 1, the model demonstrated high precision for the wetland class, but slightly lower recall, indicating some mis-classifications. However, the overall accuracy was strong, capturing nearly 94% of cases correctly. Scenario 2 showed improved precision and recall for both wetland and non-wetland classes, resulting in an overall accuracy of 93.5%. Integrating landcover products in Scenario 3 further enhanced the model’s performance, achieving an overall accuracy of 93.5%. The multi-classification in Scenario 4 showed the model’s ability to perform across different wetland types, with an overall accuracy of 88.2%. These results underscore the model’s effectiveness in accurately classifying coastal wetland areas under diverse remote sensing scenarios, highlighting its potential for practical applications in wetland mapping and ecological research. The study’s findings provide valuable insights into the efficacy of different data combinations in enhancing coastal wetland mapping accuracy, contributing to the understanding of wetland ecosystems and their environmental significance

References

Acreman, M., Holden, J., 2013. How wetlands affect floods. *Wetlands*, 33, 773–786.

Adam, E., Mutanga, O., Rugege, D., 2010. Multispectral and hyperspectral remote sensing for identification and mapping of wetland vegetation: a review. *Wetlands ecology and management*, 18, 281–296.

Agboola, G., Beni, L. H., 2024. Geospatial insights: Unraveling howard landslide suspectibility. *IGARSS 2024-2024 IEEE International Geoscience and Remote Sensing Symposium*, IEEE, 3014–3017.

Ahmed, O. S., Franklin, S. E., Wulder, M. A., White, J. C., 2015. Characterizing stand-level forest canopy cover and height using Landsat time series, samples of airborne LiDAR, and the Random Forest algorithm. *ISPRS Journal of Photogrammetry and Remote Sensing*, 101, 89–101.

Anokye, M., Fawakherji, M., Hashemi-Beni, L., 2024. Flood resilience through advanced wetland prediction. *IGARSS 2024-2024 IEEE International Geoscience and Remote Sensing Symposium*, IEEE, 5516–5520.

Blay, J., Fawakherji, M., Hashemi-Beni, L., 2024. Flood impact risk mapping in settlement areas from a 3d perspective: A case study of hurricane matthew. *IGARSS 2024-2024 IEEE International Geoscience and Remote Sensing Symposium*, IEEE, 3939–3942.

Bwangoy, J.-R. B., Hansen, M. C., Roy, D. P., De Grandi, G., Justice, C. O., 2010. Wetland mapping in the Congo Basin using optical and radar remotely sensed data and derived topographical indices. *Remote Sensing of Environment*, 114(1), 73–86.

Carle, M. V., 2011. Estimating wetland losses and gains in coastal North Carolina: 1994–2001. *Wetlands*, 31, 1275–1285.

Childers, D. L., Boyer, J. N., Davis, S. E., Madden, C. J., Rudnick, D. T., Sklar, F. H., 2006. Relating precipitation and water management to nutrient concentrations in the oligotrophic “upside-down” estuaries of the Florida Everglades. *Limnology and Oceanography*, 51(1part2), 602–616.

Chust, G., Galparsoro, I., Borja, A., Franco, J., Uriarte, A., 2008. Coastal and estuarine habitat mapping, using LIDAR height and intensity and multi-spectral imagery. *Estuarine, Coastal and Shelf Science*, 78(4), 633–643.

Echiverri, L., Macdonald, S. E., 2019. Utilizing a topographic moisture index to characterize understory vegetation patterns in the boreal forest. *Forest Ecology and Management*, 447, 35–52.

Gonzalez-Perez, A., Abd-Elrahman, A., Wilkinson, B., Johnson, D. J., Carthy, R. R., 2022. Deep and machine learning image classification of coastal wetlands using unpiloted aircraft system multispectral images and lidar datasets. *Remote Sensing*, 14(16), 3937.

Gutzwiller, K. J., Flather, C. H., 2011. Wetland features and landscape context predict the risk of wetland habitat loss. *Ecological Applications*, 21(3), 968–982.

Halabisky, M., Miller, D., Stewart, A. J., Lorigan, D., Brasel, T., Moskal, L. M., 2022. The Wetland Intrinsic Potential tool: Mapping wetland intrinsic potential through machine learning of multi-scale remote sensing proxies of wetland indicators. *EGUsphere*, 2022, 1–19.

Harenda, K. M., Lamentowicz, M., Samson, M., Chojnicki, B. H., 2018. The role of peatlands and their carbon storage function in the context of climate change. *Interdisciplinary approaches for sustainable development goals: Economic growth, social inclusion and environmental protection*, 169–187.

Hashemi Beni, L., 2023. Instance Segmentation of LIDAR Data with Vision Transformer Model in Support Inundation Mapping Under Forest Canopy Environment. *The International Archives of the Photogrammetry, Remote Sensing and Spatial Information Sciences*, 48, 203–208.

Hashemi-Beni, L., Puthenparampil, M., Jamali, A., 2024. A low-cost IoT-based deep learning method of water gauge measurement for flood monitoring. *Geomatics, Natural Hazards and Risk*, 15(1), 2364777.

Hilburn, R. L., 2024. Coastline: Disappearing grasslands major threat to biodiversity in coastal plain of se nc. Accessed: 2024-11-04.

Hu, S., Niu, Z., Chen, Y., 2017. Global wetland datasets: a review. *Wetlands*, 37, 807–817.

Junk, W. J., de Cunha, C. N., 2005. Pantanal: a large South American wetland at a crossroads. *Ecological Engineering*, 24(4), 391–401.

Kalacska, M., Chmura, G., Lucanus, O., Bérubé, D., Arroyo-Mora, J., 2017. Structure from motion will revolutionize analyses of tidal wetland landscapes. *Remote Sensing of Environment*, 199, 14–24.

Kirwan, M. L., Megonigal, J. P., 2013. Tidal wetland stability in the face of human impacts and sea-level rise. *Nature*, 504(7478), 53–60.

Larson, J., Lidberg, W., Ågren, A. M., Laudon, H., 2022. Predicting soil moisture conditions across a heterogeneous boreal catchment using terrain indices. *Hydrology and Earth System Sciences*, 26(19), 4837–4851.

Li, X., McCarty, G. W., Du, L., Lee, S., 2020. Use of topographic models for mapping soil properties and processes. *Soil Systems*, 4(2), 32.

Lin, C., 2019. Improved derivation of forest stand canopy height structure using harmonized metrics of full-waveform data. *Remote Sensing of Environment*, 235, 111436.

Mainali, K., Evans, M., Saavedra, D., Mills, E., Madsen, B., Minnemeyer, S., 2023. Convolutional neural network for high-resolution wetland mapping with open data: Variable selection and the challenges of a generalizable model. *Science of the Total Environment*, 861, 160622.

Mainali, K., Evans, M., Saavedra, D., Mills, E., Minnemeyer, S., n.d. Convolutional Neural Network for High-Resolution Wetland Mapping with Open Data: Model Transferability and Predictor's Role. *Available at SSRN 4165348*.

Maxwell, A. E., Warner, T. A., Strager, M. P., 2016. Predicting palustrine wetland probability using random forest machine learning and digital elevation data-derived terrain variables. *Photogrammetric Engineering & Remote Sensing*, 82(6), 437–447.

Merrick, M. J., Koprowski, J. L., Wilcox, C., 2013. Into the third dimension: benefits of incorporating LiDAR data in wildlife habitat models. *USDA Forest Service Proc*, 67, 389–395.

Michener, W. K., Blood, E. R., Bildstein, K. L., Brinson, M. M., Gardner, L. R., 1997. Climate change, hurricanes and tropical storms, and rising sea level in coastal wetlands. *Ecological applications*, 7(3), 770–801.

Mitra, S., Wassmann, R., Vlek, P. L., 2005. An appraisal of global wetland area and its organic carbon stock. *Current science*, 88(1), 25–35.

Mohamedou, C., Korhonen, L., Eerikäinen, K., Tokola, T., 2019. Using LiDAR-modified topographic wetness index, terrain attributes with leaf area index to improve a single-tree growth model in south-eastern Finland. *Forestry: An International Journal of Forest Research*, 92(3), 253–263.

Mohtashami, S., Eliasson, L., Hansson, L., Willén, E., Thierfelder, T., Nordfjell, T., 2022. Evaluating the effect of DEM resolution on performance of cartographic depth-to-water maps, for planning logging operations. *International Journal of Applied Earth Observation and Geoinformation*, 108, 102728.

Nagelkerken, I., Blaber, S., Bouillon, S., Green, P., Haywood, M., Kirton, L., Meynecke, J.-O., Pawlik, J., Penrose, H., Sasekumar, A. et al., 2008. The habitat function of mangroves for terrestrial and marine fauna: a review. *Aquatic botany*, 89(2), 155–185.

New Hanover County, 2024. Environmental stewardship. Accessed: 2024-11-04.

Ouyang, Z., Becker, R., Shaver, W., Chen, J., 2014. Evaluating the sensitivity of wetlands to climate change with remote sensing techniques. *Hydrological Processes*, 28(4), 1703–1712.

Port City Daily, 2023. Nhc has 'cooked the golden goose,' conservationists push to protect biodiversity hotspot. Accessed: 2024-11-04.

Pricope, N., Halls, J., Dalton, E., Minei, A., Chen, C., Wang, Y., 2024. Precision Mapping of Coastal Wetlands: An Integrated Remote Sensing Approach Using Unoccupied Aerial Systems Light Detection and Ranging and Multispectral Data. *J. Remote Sens*, 4, 0169.

Rapinel, S., Hubert-Moy, L., Clément, B., 2015. Combined use of LiDAR data and multispectral earth observation imagery for wetland habitat mapping. *International journal of applied earth observation and geoinformation*, 37, 56–64.

Riihimäki, H., Kemppinen, J., Kopeckỳ, M., Luoto, M., 2021. Topographic wetness index as a proxy for soil moisture: The importance of flow-routing algorithm and grid resolution. *Water Resources Research*, 57(10), e2021WR029871.

Tiner, R. W., 2016. *Wetland indicators: A guide to wetland formation, identification, delineation, classification, and mapping*. CRC press.

Torres-Bejarano, F., Arteaga-Hernández, F., Rodríguez-Ibarra, D., Mejía-Ávila, D., González-Márquez, L., 2021. Water quality assessment in a wetland complex using Sentinel 2 satellite images. *International Journal of Environmental Science and Technology*, 18(8), 2345–2356.

Wasehun, E. T., Beni, L. H., Di Vittorio, C. A., Zarzar, C. M., Young, K. R., 2025. Comparative analysis of Sentinel-2 and PlanetScope imagery for chlorophyll-a prediction using machine learning models. *Ecological Informatics*, 85, 102988.